Control and estimation strategies for pneumatic drives with partial position information

Contact:

Automation and Control Institute (ACIN)
Vienna University of Technology
Gusshausstrasse 27-29/E376
1040 Vienna, Austria

Internet: www.acin.tuwien.ac.at
E-mail: office@acin.tuwien.ac.at
Phone: +43 1 58801 37601
Fax: +43 1 58801 37699

Control and Estimation Strategies for Pneumatic Drives with Partial Position Information

Andreas Pfeffer[a,1,*], Tobias Glück[b,2], Florian Schausberger[a], Andreas Kugi[a,1]

[a] *Automation and Control Institute, TU Wien, Vienna, Austria*
[b] *Complex Dynamical Systems, Austrian Institute of Technology, Vienna, Austria*

Abstract

Flexibility in production demands for flexible components which automatically adjust to new operating conditions. Pneumatic drives are often used in various industrial applications, e.g., for point-to-point movements. The motion characteristics is typically set up by manual tuning. Therefore, changes in the production lines typically require costly manual readjustments. This can be avoided by using a robust, but expensive servo-control with pressure sensors and a full-stroke position sensor. In this paper, we propose a cost-efficient and flexible alternative by combining classical pressure sensors with cheap partial position sensors at the end strokes to estimate the parameters of the mechanical system of the drive. This allows to readjust the motion characteristics in real time. Another costly issue is the limitation of the lifetime of the drive, when varying loads lead to large impacts at the stroke ends. To increase the lifetime, a novel non-overshooting trajectory planning algorithm is presented in this work. The overall control concept is implemented on two lab test benches and the experimental results prove its excellent performance and robustness with respect to changing operating conditions.

Keywords: Pneumatic systems; disturbance rejection; parameter estimation; feedforward control; trajectory planning.

1. Introduction

In today's manufacturing plants, many tasks are performed with pneumatics, see, e.g., [1]. One of the standard applications are simple endpoint-to-endpoint movements. Pneumatic drives are ideally suited to such tasks because they feature low investment costs and a high power density, see, e.g., [2, 3, 4]. In general, two approaches are used to control the movement of pneumatic drives.

In the majority of cases, the pneumatic drives are equipped with simple open-loop switching strategies and throttle valves without any further sensors. The lack of measurement information makes this approach cheap, but quite inflexible in terms of operating conditions. The typical fields of application are endpoint-to-endpoint movements, where mechanical end-stops are employed to limit the movement of the drive. A speed limitation is realized by manual tuning of the throttle valves, while built-in damping elements (for example elastomer's, pneumatic dampers,...) in the pneumatic drive reduce the impact energy at the mechanical end-stops. These damping measures are intended to ensure a so called soft landing of the piston and thus increase the lifetime of the drive. Beside the extra effort of including such dampers in the construction of the drive, some of these technologies require manual adjustments and thus cause additional costs when bringing the system into service. Often these pneumatic drives are oversized and do not operate at high efficiency, see, e.g., [5], which of course entails higher running costs. To sum it up, the main drawbacks of these simple pneumatic drives are the inflexibility due to the lack of sensors and the typically higher operational costs. The initial cost savings may finally result in high follow-up costs because also every change in the environment of the drive demands for new adjustments, e.g., of the throttle valves.

The second state-of-the-art approach is classical servo-control, see, e.g., [6, 7, 8, 9, 10, 11, 12, 13], which allows to control the position of the piston along a desired trajectory. Clearly, this requires full-stroke position sensors. An overview of different types of servo-control strategies can be found in [14, 15]. Nowadays, often modern non-linear control strategies like exact linearization, see, e.g., [15, 16], sliding mode control, see, e.g., [3, 7, 9, 10, 17, 18], or immersion and invariance concepts [19] are applied. Typically an expensive, e.g., 5-port/3-way, proportional valve is used to control the drive, which leads to a single-input-single-output system for position control, see, e.g., [4, 7, 18, 20, 21]. A pure feedback position controller can then be used for the drive. But, even if measurable, the chamber pressures cannot be controlled, since the only control input is used for the position control. This in combination with the typical leakage flows of such proportional valves results in a lower

*Corresponding author
[1] (e-mail: {pfeffer,kugi}@acin.tuwien.ac.at)
[2] (e-mail: Tobias.Glueck@ait.ac.at)

Post-print version of the article: A. Pfeffer, T. Glueck, F. Schausberger, and A. Kugi, "Control and estimation strategies for pneumatic drives with partial position information", *Mechatronics*, vol. 50, pp. 259–270, 2018. DOI: doi.org/10.1016/j.mechatronics.2017.09.012
The content of this post-print version is identical to the published paper but without the publisher's final layout or copy editing.

efficiency due to high chamber pressures, see, e.g., [2, 22]. An attractive alternative is given by two pneumatic half-bridges equipped with two, e.g., 2-port/2-way switching valves each. Beside the cost savings due to the elimination of the leakage flows, this approach allows to separately control the chamber pressure or the actuator force and the piston position, see, e.g., [1, 3, 23, 24, 25, 26, 27, 28]. The combination of a full-stroke position sensor with pressure sensors and two half bridges is the most flexible approach, but also the one with the highest equipment costs. In literature, several works can be found which reduce the equipment costs of servo-controlled drives, e.g., by omitting the chamber pressure sensors, see, e.g., [29]. Alternatively, an observer can be designed to estimate both chamber pressures, see, e.g., [29, 30]. Note that for all these approaches still a full-stroke position sensor is needed. Typically this is cost effective for short-stroke drives where cheap position measurement systems are available. For drives with long strokes, the price of a full-stroke position sensor is much higher compared to the costs of two pressure sensors.

Nowadays, the major challenge of pneumatic drives is to reduce the overall running costs, see, e.g., [1, 22]. The main cost drivers are air consumption and maintenance. The air consumption can be curbed by avoiding leakage flows and by reducing at least the sum of the chamber pressures, while the maintenance costs can be kept small by a flexible and robust control concept.
Moreover in industrial applications, pneumatic drives are often faced with varying or not exactly known operating conditions. A typical example is the supply pressure. Of course, the supply pressure level at the compressor power station can be chosen within certain limits and usually different service units with mechanical pressure controllers are used to regulate the supply pressure level in a manufacturing plant. But due to the costs of the service units, they typically supply a large number of pneumatic components. This in combination with different pipe diameters and pipe lengths to the valves and to the actuators can lead to varying supply pressure levels and sometimes even to significant pressure drops at the pneumatic components. For standard applications, the varying supply pressure may thus lead to unintended changes in the clock speed of the production line or may result in harmful impacts of the piston on the stroke ends. In [31] a novel robust approach for endpoint-to-endpoint movements is presented, which tackles the systematic handling of such pressure drops and represents the basis for the current work. For this approach, the drive is equipped with leakage free switching valves and a sensor concept comprising pressure sensors and two cheap non-contacting position sensors with short measurement range placed near each stroke end. Compared to a combination of a proportional valve with only a low cost full-stroke position sensor for a classical servo control, the costs of the utilized valves and sensors are about 20 percent smaller. When the servo control also comprises pressure sensors, the cost advantage of the presented approach rises up to more than 30 percent. The presented control approach allows to suppress supply pressure drops even during the movement of the piston and to reduce the overall air consumption compared to the classical approaches. In a nutshell, the movement is realized by using chamber pressure trajectory control. The desired pressure trajectories are planned by utilizing the differential flatness property of the system. This also allows to systematically compute a feedforward controller for the valves in real time, which offers the possibility to account for the measurable supply pressure drops. An additional feedback controller is used to ensure robustness with respect to model uncertainties and disturbances. Apart from the supply pressure also the real moving mass of the drive is not always exactly known. Moreover, it is well known that the friction of the system may exhibit large variations during operation depending on the application. For most model-based control applications, the knowledge of the exact mass is important to achieve a high control performance and accuracy. In literature, different estimation strategies for pneumatic drives can be found, see, e.g., [19, 29]. The concept of [19] is based on an adaptive immersion and invariance approach, see, e.g., [32], where the friction force is estimated online. The limitation is that the mass has to be known exactly for accurate estimations. In the latter approach from [29], a least-squares estimation is proposed. The drawback of this approach is that the Coulomb friction parameter must be known in advance for online estimation of the mass and of the viscous friction parameter.
In the following, an extension of [31] to overcome the challenges concerning varying parameters is presented. To estimate the mass and the friction of the system simultaneously an online parameter estimation algorithm is derived. The algorithm presented in this work uses two identical estimators in parallel to combine fast convergence with high robustness with respect to noise. The two estimators are based on recursive least-squares algorithms, see, e.g., [33]. Investigations concerning the influence of the mounting orientation of the drive and of the sensor noise lead to a tailored estimation concept. This parameter estimator offers new possibilities for the control strategy presented in [31]. First, the knowledge of the actual parameters allows to update the flatness-based feedforward controller of the endpoint-to-endpoint motion planning. Second, instead of the robust but not very precise impedance control presented in [31] a combination of feedforward and position control can be used in the region where position information is available at the stroke ends. For this, a tailored non-overshooting trajectory planning algorithm is developed.

The paper is structured as follows: In Section 2, the experimental setup is introduced and its mathematical model is derived. Based on this model, the overall control strategy is presented in Section 3 and the parameter estimation algorithm is given in Section 4. Finally in Section 5, measurements are shown to validate the feasibility of the proposed

Post-print version of the article: A. Pfeffer, T. Glueck, F. Schausberger, and A. Kugi, "Control and estimation strategies for pneumatic drives with partial position information", *Mechatronics*, vol. 50, pp. 259–270, 2018. DOI: doi.org/10.1016/j.mechatronics.2017.09.012
The content of this post-print version is identical to the published paper but without the publisher's final layout or copy editing.

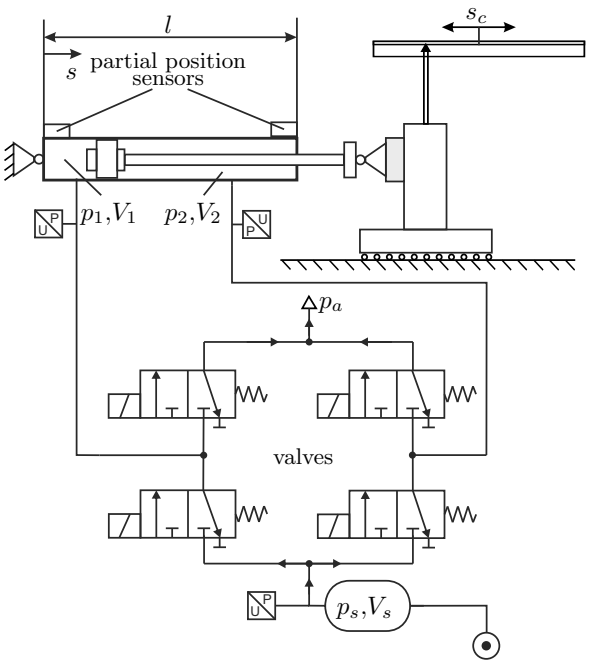

Figure 1: Schematic of the pneumatic linear drive containing the four fast switching valves, the position sensors, and the pressure sensors for a horizontal mounting of the drive.

concepts. The paper closes with some short conclusions.

2. Experimental Setup and Mathematical Model

In the following, the experimental setup is described and the corresponding mathematical model is derived.

2.1. Experimental Setup

A schematic of the system under investigation is shown in Figure 1. A pneumatic drive consisting of a differential cylinder and four fast 2-port/2-way switching valves is considered. Two short position sensors are mounted near each stroke end. For the estimation strategy as well as for the position control concept, three pressure sensors for the supply pressure and the two chamber pressures are required. In addition, a full-stroke position measurement sensor is mounted for validation purposes only.

2.2. Mathematical Model

An average model of the pneumatic drive with PWM (pulse-width modulation)-controlled switching valves is presented in [31]. For the reason of completeness, it will be shortly repeated in the following. Let $\bar{\xi}$ denote an average value of the variable ξ over a modulation period T, i.e.,

$$\bar{\xi} = \frac{1}{T}\int_{t-T}^{t} \xi(\tau)\mathrm{d}\tau. \tag{1}$$

Then the average model of the PWM-controlled pneumatic drive reads as [31]

$$\ddot{\bar{s}} = \frac{1}{m}\Big(F_f\big(\dot{\bar{s}}\big) + F_p\big(\bar{p}_1,\bar{p}_2\big) + F_g + F_a\Big) \tag{2a}$$

$$\dot{\bar{p}}_i = \frac{\kappa}{V_i(\bar{s})}\left((-1)^i A_i \dot{\bar{s}}\bar{p}_i + R\theta_g \dot{\bar{m}}_i\right),\ i \in \{1,2\}\ . \tag{2b}$$

Coulomb and viscous friction is modelled by $F_f(\dot{\bar{s}}) = -c\tanh(\dot{\bar{s}}/\varepsilon) - d\dot{\bar{s}}$ with the Coulomb friction coefficient $c > 0$, the parameter $0 < \varepsilon \ll 1$, and the viscous friction coefficient d. Moreover, $F_p(\bar{p}_1,\bar{p}_2) = \bar{p}_1 A_1 - \bar{p}_2 A_2$ denotes the pressure force, with the effective areas A_1 and A_2, and $F_a = p_a(A_2 - A_1)$ is the pressure force offset due to the (constant) ambient pressure p_a. Depending on the mounting orientation, the gravitational force takes the form $F_g = -mg\sin(\varphi)$. Here, m denotes the overall moving mass, g is the gravitational acceleration, and φ is the angle of the mounting orientation relative to the effective line of g. In (2b), κ denotes the specific heat ratio of air, $V_1(\bar{s}) = A_1\bar{s} + V_{1,0}$ and $V_2(\bar{s}) = A_2(l-\bar{s}) + V_{2,0}$ are the chamber volumes with dead volumes $V_{1,0}$ and $V_{2,0}$, l is the maximum stroke length, and R denotes the specific gas constant. The gas temperature θ_g is assumed to be constant and equal to the ambient temperature. The mass flows $\dot{\bar{m}}_i$, $i \in \{1,2\}$ read as

$$\dot{\bar{m}}_1 = C_{\max}\big(\Gamma_{1s}(\bar{p}_1)\chi_{1s} - \Gamma_{a1}(\bar{p}_1)\chi_{a1}\big) \tag{2c}$$

$$\dot{\bar{m}}_2 = C_{\max}\big(\Gamma_{2s}(\bar{p}_2)\chi_{2s} - \Gamma_{a2}(\bar{p}_2)\chi_{a2}\big), \tag{2d}$$

with conductance $C_{\max}$, duty ratios $\chi_{ij} \in [0,1]$, $ij \in \{1s,a1,2s,a2\}$ of the pulse-width modulated conductances, and

$$\Gamma_{ij}(\bar{p}_i) = \rho_0 \bar{p}_j \Psi\left(\Pi_{ij}\right), \quad ij \in \{1s,a1,2s,a2\}\ , \tag{2e}$$

where ρ_0 denotes the technical density of air, $\bar{p}_s$ is the supply pressure, and $\Pi_{ij} = \bar{p}_i/\bar{p}_j$ is the pressure ratio. In (2e), $\Psi\left(\Pi_{ij}\right)$ refers to the flow-through function, see, e.g., [14, 23],

$$\Psi\left(\Pi_{ij}\right) = \begin{cases} \sqrt{1 - \left(\frac{\Pi_{ij}-\Pi_c}{1-\Pi_c}\right)^2} & \text{for} \quad \Pi_{ij} \geq \Pi_c \\ 1 & \text{for} \quad \Pi_{ij} < \Pi_c\ , \end{cases} \tag{2f}$$

with the critical pressure ratio Π_c.

3. Control Strategy

A control strategy for the extension and retraction of the piston rod is presented. The strategy is schematically depicted in Figure 2. The light blue background indicates that except for a short range near the stroke ends only pressure information is available. Starting at an end stop, the piston with the load is moved by pressure control towards the opposite stroke end into the corresponding position measurement range. In the position measurement range,

Post-print version of the article: A. Pfeffer, T. Glueck, F. Schausberger, and A. Kugi, "Control and estimation strategies for pneumatic drives with partial position information", *Mechatronics*, vol. 50, pp. 259–270, 2018. DOI: doi.org/10.1016/j.mechatronics.2017.09.012
The content of this post-print version is identical to the published paper but without the publisher's final layout or copy editing.

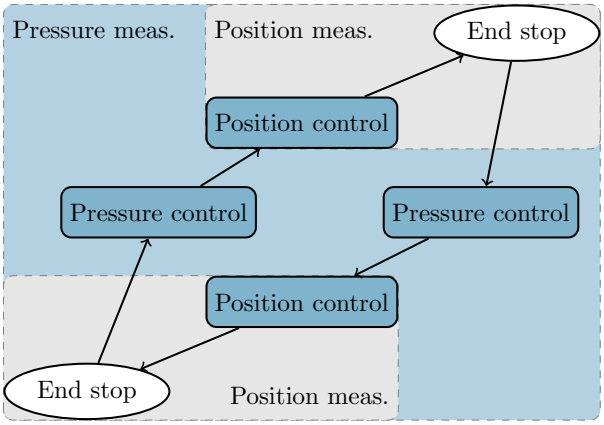

Figure 2: Flow chart of the overall control strategy.

position control is activated. Both controllers consist of a flatness-based feedforward controller and a feedback controller. Smooth trajectories from one end stop to the other are planned. When the piston enters the position measurement range, the position trajectory is adapted to the new measured conditions with respect to velocity and acceleration and a non-overshooting position trajectory to the end stop is planned. This is necessary because the pressure controller does not guarantee that the position, velocity, and acceleration of the piston coincide with the reference trajectory due to model uncertainties and disturbances. In addition, inside the position measurement range a master-slave least-squares identification procedure is used to estimate the moving mass and the friction. The model-based pressure and position control algorithms are parametrized by these estimated parameters. If errors occur in the range without position information, a feedforward controller is activated to ensure a piston movement into the right direction until the corresponding measurement range is reached.

In [31], the soft landing of the pneumatic piston at the end stops is realized using an impedance control algorithm in the position measurement range. This approach works quite well for a given set of parameters. Furthermore, in combination with the pressure control even large uncertainties concerning the thermodynamic part of the model can be handled. The proposed impedance control concept turns out to be robust with respect to moderate uncertainties in the mass and the friction parameters. However, in order to ensure the same mass-spring-damper behaviour, either mass shaping or a variation of the controller parameters (spring and damper constants) is needed. Note that mass shaping requires direct force measurement. In the following, a combination of a MIMO position controller and a tailored trajectory planning is proposed to allow for larger variations of the mass and the friction parameters and simultaneously guarantee a smooth landing of the drive at the end stops.

3.1. Flatness-based Parametrization

The mathematical model (2) is differentially flat with outputs $w_1 = \bar{s}$ and $w_2 = \bar{p}_1 + \bar{p}_2$, see, e.g., [4, 34]. Thus, all states and control inputs can be parametrized in terms of the flat outputs w_1, w_2, and their time derivatives. The relative degrees of w_1 and w_2 with respect to the (virtual) control inputs $\bar{m}_1$ and $\bar{m}_2$ are $r_1 = 3$ and $r_2 = 1$. Subsequently, an upper index d always refers to the corresponding desired reference trajectory. The state parametrization can be obtained from (2a) in form

$$\bar{s}^d = w_1^d \tag{3a}$$

$$\dot{\bar{s}}^d = \dot{w}_1^d \tag{3b}$$

$$\bar{p}_1^d = \psi_1\big(w_2^d, \dot{w}_1^d, \ddot{w}_1^d\big) = -\frac{1}{A_1 + A_2}\big(- m\ddot{w}_1^d + F_f\big(\dot{w}_1^d\big) - A_2 w_2^d + F_a + F_g\big) \tag{3c}$$

$$\bar{p}_2^d = \psi_2\big(w_2^d, \dot{w}_1^d, \ddot{w}_1^d\big) = w_2^d + \frac{1}{A_1 + A_2}\big(- m\ddot{w}_1^d + F_f\big(\dot{w}_1^d\big) - A_2 w_2^d + F_a + F_g\big)\,. \tag{3d}$$

Moreover, the parametrization of the control inputs $\bar{m}_1$ and $\bar{m}_2$ result from (2b) and directly constitute the feedforward controller for the desired reference trajectories $w_1^d = \bar{s}^d$ and $w_2^d = \bar{p}_1^d + \bar{p}_2^d$. Finally, the real control inputs $\chi_{1s}, \chi_{2s}, \chi_{a1}, \chi_{a2}$ result from (2c), (2d) by avoiding direct flows between the corresponding inlet and outlet valves.

3.2. Trajectory Planning

As already mentioned before, a nominal trajectory for the piston is planned which connects the two end stops. For this, polynomial reference trajectories of class $\mathcal{C}^{r_1}$ and $\mathcal{C}^{r_2}$ are chosen for the flat outputs w_1^d and w_2^d. The trajectory for w_1^d simply results from its boundary conditions. These are the transition time, the maximum piston stroke and the requirement of zero velocity and zero acceleration at the beginning and the end of the trajectory. For the second flat output of the system a tailored approach, where two polynomials are connected, is used. The resulting additional degrees of freedom allow to reduce the maximum inputs needed to realize the chosen trajectories of the system. For more information on the trajectory planning, see [31].

When the piston enters the position measurement range, a new non-overshooting position trajectory w_1^d is proposed in the following. It is based on the work of [35, 36] and [37]. For the sake of brevity, only the trajectory for the extension of the piston is considered. Due to the fact that the feedforward and the pressure control move the piston with a positive velocity and a negative acceleration into the position measurement range, only negative accelerations are requested to smoothly move the piston to the end stop. The trajectory for the retraction can be derived analogously, only the signs of the corresponding derivatives must be changed. In order to obtain a non-overshooting

Post-print version of the article: A. Pfeffer, T. Glueck, F. Schausberger, and A. Kugi, "Control and estimation strategies for pneumatic drives with partial position information", *Mechatronics*, vol. 50, pp. 259–270, 2018. DOI: doi.org/10.1016/j.mechatronics.2017.09.012
The content of this post-print version is identical to the published paper but without the publisher's final layout or copy editing.

position trajectory w_1^d, an acceleration trajectory with four phases is used. The acceleration trajectory consists of two constant segments and two sine-squared blend segments to yield a trajectory of class $\mathcal{C}^3$. In the nominal case (Case 1), the mathematical formulation reads as

$$\ddot{w}_1^d = \begin{cases} a_0 & \mathcal{J}_0 = [t_0, t_1] \\ a_1(t) & \mathcal{J}_1 = [t_1, t_2] \\ a_2 & \mathcal{J}_2 = [t_2, t_3] \\ a_3(t) & \mathcal{J}_3 = [t_3, t_f] \end{cases} \tag{4a}$$

with

$$a_1(t) = a_0 - (a_0 - a_2)\sin^2\left(\frac{\pi}{2\tilde{t}_1}(t - t_1)\right) \tag{4b}$$

$$a_3(t) = a_2 - a_2\sin^2\left(\frac{\pi}{2\tilde{t}_3}(t - t_3)\right) \tag{4c}$$

and $\tilde{t}_i = t_{i+1} - t_i, i = 0, \ldots, 3$ and the final time $t_4 = t_f$. The time when the piston enters the position measurement range is set to $t_0 = 0$. There are six parameters to be determined, i.e., $a_0, a_2, \tilde{t}_0, \tilde{t}_1, \tilde{t}_2$, and $\tilde{t}_3$. The first parameter a_0 is given by the initial acceleration[3]

$$\ddot{w}_1^d(t_0) = a_0 = \ddot{s}(t_0)\ . \tag{5a}$$

The trajectories $\dot{w}_1^d(t)$ and $w_1^d(t)$ are obtained by integrating (4) once and twice, respectively. In view of the desired soft landing the change of the velocity Δv^d during the time period $t_f - t_0$ follows as

$$\begin{aligned} \Delta v^d &= \dot{w}_1^d(t_f; a_0, a_2, \tilde{t}_0, \tilde{t}_1, \tilde{t}_2, \tilde{t}_3) - \dot{w}_1^d(t_0; a_0, a_2, \tilde{t}_0, \tilde{t}_1, \tilde{t}_2, \tilde{t}_3) \\ &= -v_0 = -\dot{s}(t_0), \end{aligned} \tag{5b}$$

while the position change is given by

$$\Delta s^d = w_1^d(t_f; a_0, a_2, \tilde{t}_0, \tilde{t}_1, \tilde{t}_2, \tilde{t}_3) = s^d(t_f) - s_0. \tag{5c}$$

For simplicity, $w_1^d(t_0) = s_0 = 0$ is chosen as starting position because the position offset can always be shifted to the measured position value. The trajectory automatically fulfils the boundary conditions $\dot{w}_1^d(t_f) = 0$ and $\ddot{w}_1^d(t_f) = 0$ because of (4). In addition to (5b) and (5c) the trajectory should not exceed a minimum acceleration $\ddot{s}_{\min}$ and a minimum jerk $\dddot{s}_{\min}$ which is ensured by

$$a_2 = \eta \ddot{s}_{\min} \tag{5d}$$

and

$$\tilde{t}_1 = \frac{\pi(a_2 - a_0)}{2\eta \dddot{s}_{\min}}, \quad \tilde{t}_3 = \frac{\pi a_2}{2\eta \dddot{s}_{\min}} \tag{5e}$$

[3]Of course the initial acceleration cannot be measured. Due to the active pressure control before the piston enters the position measurement range, the acceleration of the piston is approximately $\ddot{w}_1^d$. Therefore, $\ddot{w}_1^d(t_0)$ is taken from the flatness-based trajectory planning.

with $\eta \in [0,1]$. The remaining parameters $\tilde{t}_0$ and $\tilde{t}_2$ follow from the conditions (5b) and (5c).

In the following, six cases resulting from different initial conditions $\ddot{s}(t_0)$ and $\dot{s}(t_0)$ will be distinguished. The corresponding trajectories are depicted in Figs. 3 to 8, where the gray arrows indicate the remaining degrees of freedom used to fulfil the requirements (5). Case 1 in Fig. 3 represents the nominal case, where the parameters $a_0, a_2, \tilde{t}_1$, and $\tilde{t}_3$ are fixed by (5a), (5d), and (5e). When the piston shows a lower entry velocity, less deceleration is needed. As a result, $\tilde{t}_2$ will be reduced. When $\tilde{t}_2$ reaches zero the trajectory changes to Case 2, see Fig. 4. Now condition (5d) does no longer hold and a_2 is a new degree of freedom instead of $\tilde{t}_2$. As a consequence $a_2 < a_0$ must hold. A further reduction of the entry velocity leads to Case 3. Here, a_2 is set to $a_2 = a_0$ and the two remaining degrees of freedom are $\tilde{t}_0$ and $\tilde{t}_3$. Fig. 5 shows the corresponding trajectory. This case is valid until $\tilde{t}_0 = 0$. When the entry velocity is further reduced (Case 4) then $a_2 > a_0$ is needed to fulfil all requirements and so the sign for the first blend segment changes, see Fig. 6.
For some given entry conditions, Case 1 does not meet the requirements because, e.g., the entry velocity is too high, which is why another change in the trajectory planning must be performed, which is shown in Fig. 7. First, the time span $\tilde{t}_0$ is set to zero and the new degree of freedom is a_2. Clearly, in this case a deceleration can be demanded which cannot be realized with the given equipment. But it is the best one can do under the given system constraints. Finally, a further increase in the entry velocity leads to Case 6, shown in Fig. 8. In this case, the maximum deceleration as well as the minimum jerk of (5e) are chosen as additional degrees of freedom. In a compact form, the six cases can be summarized as follows:

Case 1: The intervals $\mathcal{J}_0$–$\mathcal{J}_3$ are present. Unknown are $a_0, a_2, \tilde{t}_0, \tilde{t}_1, \tilde{t}_2$, and $\tilde{t}_3$. They result directly from (5).

Case 2: The intervals $\mathcal{J}_0, \mathcal{J}_1$ and $\mathcal{J}_3$ are present and $\tilde{t}_2$ is set to zero. Unknown are $a_0, a_2, \tilde{t}_0, \tilde{t}_1$, and $\tilde{t}_3$. They result directly from (5a)-(5c) and (5e).

Case 3: The intervals $\mathcal{J}_0$ and $\mathcal{J}_3$ are present and again $\tilde{t}_2$ is set to zero. Unknown are $a_0, a_2, \tilde{t}_0, \tilde{t}_1$, and $\tilde{t}_3$. They result directly from (5a)-(5c), (5e), and $a_0 = a_2$.

Case 4: The intervals $\mathcal{J}_1, \mathcal{J}_2$ and $\mathcal{J}_3$ are present and $\tilde{t}_0$ is set to zero. Unknown are $a_0, a_2, \tilde{t}_1, \tilde{t}_2$, and $\tilde{t}_3$. They result directly from (5a)-(5c), and (5e), with $|a_2| < |a_0|$.

Case 5: The intervals $\mathcal{J}_1, \mathcal{J}_2$ and $\mathcal{J}_3$ are present and $\tilde{t}_0$ is set to zero. Unknown are $a_0, a_2, \tilde{t}_1, \tilde{t}_2$, and $\tilde{t}_3$. They result directly from (5a)-(5c), and (5e).

Case 6: The intervals $\mathcal{J}_1$ and $\mathcal{J}_3$ are present and $\tilde{t}_0$ as well as $\tilde{t}_2$ are set to zero. Unknown are $a_0, a_2, \tilde{t}_1, \tilde{t}_3$, and $\dddot{s}_{\min}$. They result directly from (5a)-(5c), and (5e).

Post-print version of the article: A. Pfeffer, T. Glueck, F. Schausberger, and A. Kugi, "Control and estimation strategies for pneumatic drives with partial position information", *Mechatronics*, vol. 50, pp. 259–270, 2018. DOI: doi.org/10.1016/j.mechatronics.2017.09.012
The content of this post-print version is identical to the published paper but without the publisher's final layout or copy editing.

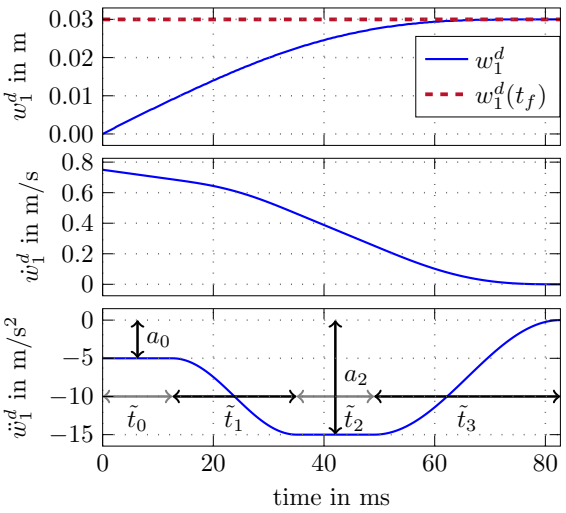

Figure 3: Position trajectory and its derivatives for Case 1.

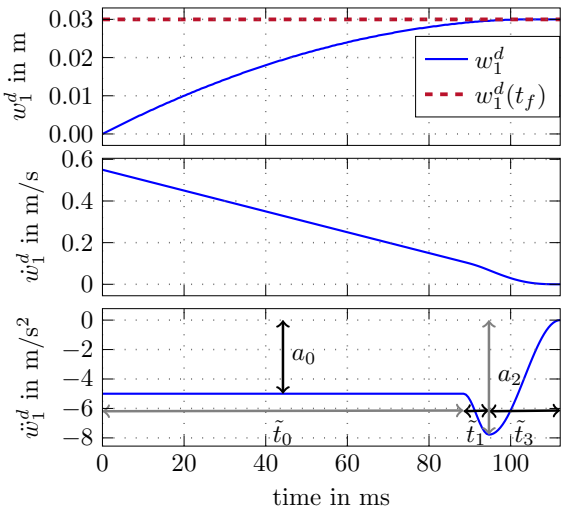

Figure 4: Position trajectory and its derivatives for Case 2.

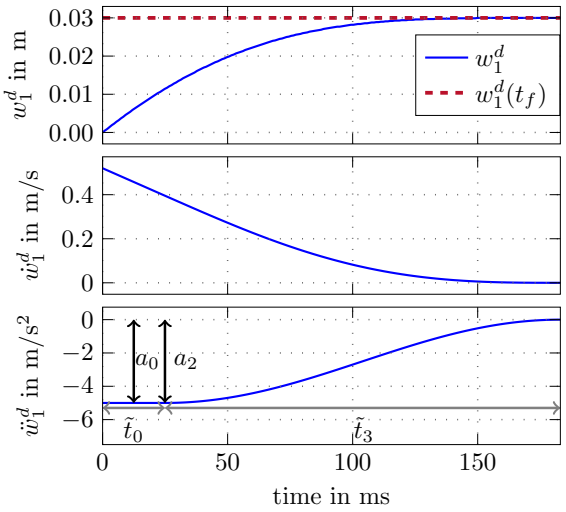

Figure 5: Position trajectory and its derivatives for Case 3.

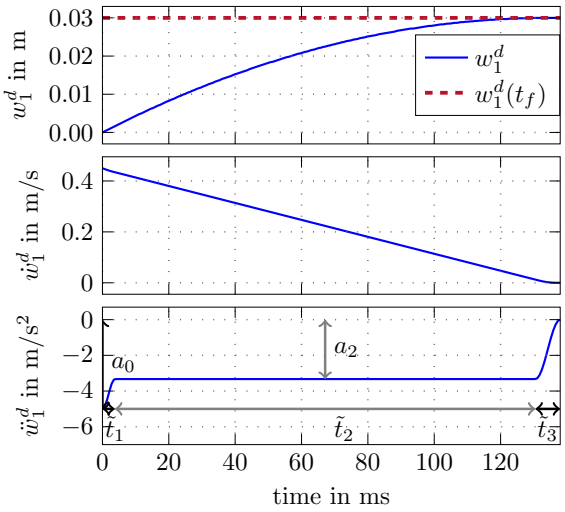

Figure 6: Position trajectory and its derivatives for Case 4.

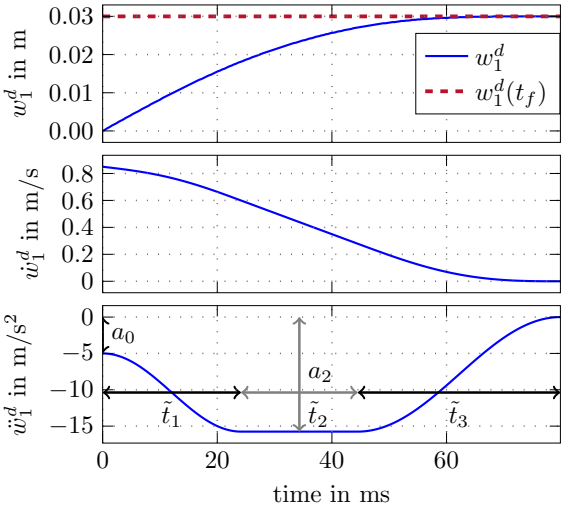

Figure 7: Position trajectory and its derivatives for Case 5.

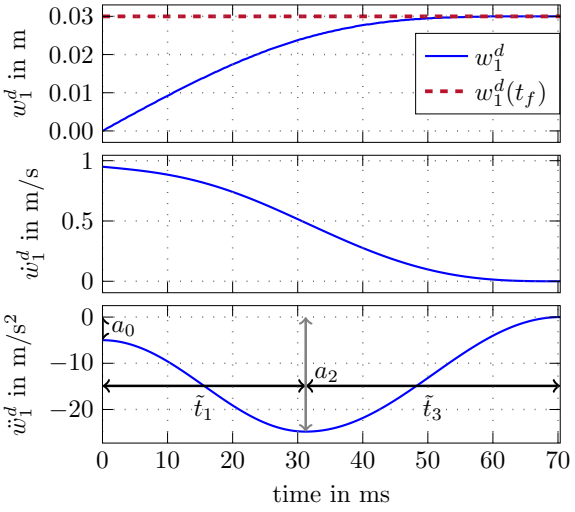

Figure 8: Position trajectory and its derivatives for Case 6.

Post-print version of the article: A. Pfeffer, T. Glueck, F. Schausberger, and A. Kugi, "Control and estimation strategies for pneumatic drives with partial position information", *Mechatronics*, vol. 50, pp. 259–270, 2018. DOI: doi.org/10.1016/j.mechatronics.2017.09.012
The content of this post-print version is identical to the published paper but without the publisher's final layout or copy editing.

The six cases are chosen according to Table 1. Note that only the extension of the piston and thus combinations of $v_0 > 0$ and $a_0 < 0$ are taken into account. This is ensured by the feedforward and pressure control. Figure 9 shows the

Initialize: $s_0 > 0, v_0 > 0, a_0 < 0$
do Case 1
  if $\tilde{t}_2 < 0$
    do Case 2
      if $|a_2| \leq |a_0|$
        do Case 3
          if $\tilde{t}_0 < 0$
            do Case 4
  else if $\tilde{t}_0 < 0$
    do Case 5
      if $\tilde{t}_2 < 0$
        do Case 6
end

Table 1: Algorithm for the position trajectory planning in the position measurement range.

distribution of the six cases for different initial conditions $v_0 \in [0.1,1.1]\text{m/s}$ and $a_0 \in [-6,0]\text{m/s}^2$. The map indicates that for high entry velocities the resulting trajectory is generated by Case 6 and for low entry velocities Case 4 is used. It can be easily seen from Fig. 8 and (4) that Case 6 holds true for all combinations of a_0 and large v_0. In Case 4, the trajectory can fulfil the requirements even with a sufficiently small a_2 and an appropriate time span $\tilde{t}_2$ also for very small entry velocities v_0. In this case, the final time t_f becomes very large. In practise, Case 4 is only used if the entry velocity is above a lower limit. For entry velocities below this limit, a constant final position $s_f = s(t_f)$ is used as reference for the position control to force the piston movement.

3.3. Pressure Control

Pure pressure control is used in the area without position information to account for uncertainties in the pneumatic subsystem, e.g., in the conductances or in the dead volumes. Feedback linearization, see, e.g., [34], applied to (2b) with outputs $y_i = \bar{p}_i$ for $i \in \{1,2\}$ yields the virtual control inputs

$$\bar{\dot{m}}_i = \frac{1}{g_i}\left(\alpha_i - f_i\right) \ , \ i \in \{1,2\}, \tag{6a}$$

with

$$f_i = \frac{\kappa}{V_i(\bar{s})}(-1)^i A_i \bar{\dot{s}} \bar{p}_i \ , \quad g_i = \frac{\kappa R \theta_g}{V_i(\bar{s})} \ . \tag{6b}$$

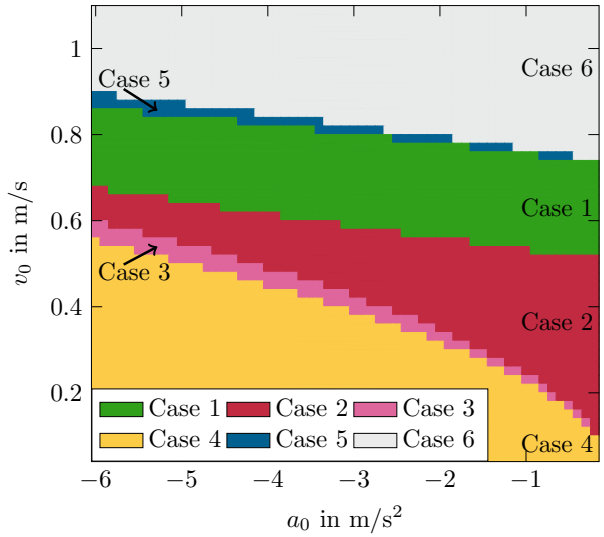

Figure 9: Distribution of the six cases for the position trajectory planning depending on the initial velocity v_0 and acceleration a_0.

The true control inputs are obtained by

$$\chi_{is} = \begin{cases} \frac{\bar{\dot{m}}_i}{C_{\max}\Gamma_{is}(\bar{p}_i)} \ , & \bar{\dot{m}}_i \geq 0 \\ 0 \ , & \bar{\dot{m}}_i < 0 \ , \end{cases} \tag{6c}$$

$$\chi_{ai} = \begin{cases} 0 \ , & \bar{\dot{m}}_i \geq 0 \\ \frac{-\bar{\dot{m}}_i}{C_{\max}\Gamma_{ai}(\bar{p}_i)} \ , & \bar{\dot{m}}_i < 0 \ . \end{cases} \tag{6d}$$

The term α_i in (6a) reads as

$$\alpha_i = \bar{\dot{p}}_i^d - a_{i,0} e_i - a_{i,1} \int_0^t e_i \, \mathrm{d}\tau \ , \tag{6e}$$

with the pressure reference trajectory $\bar{p}_i^d$ according to (3), the pressure error $e_i = \bar{p}_i - \bar{p}_i^d$, and the constant controller parameters $a_{i,j} > 0$. Application of (6) to (2b) yields a linear and exponentially stable error dynamics.

3.4. Combined Position and Pressure Control

Position control is used in the position measurement range. Feedback linearization applied to (2) with outputs w_1 and w_2 yields the virtual control inputs

$$\begin{bmatrix} \bar{\dot{m}}_1 \\ \bar{\dot{m}}_2 \end{bmatrix} = \mathbf{G}^{-1}\left(\boldsymbol{\beta} - \mathbf{f}\right) \ . \tag{7a}$$

The decoupling matrix $\mathbf{G}$ and the function $\mathbf{f}$ are given by

$$\mathbf{G} = \begin{bmatrix} \frac{A_1}{m} g_1 & -\frac{A_2}{m} g_2 \\ g_1 & g_2 \end{bmatrix}, \quad \mathbf{f} = \begin{bmatrix} \dot{F}_f + A_1 f_1 - A_2 f_2 \\ f_1 + f_2 \end{bmatrix} \ , \tag{7b}$$

with f_i and g_i, $i \in \{1,2\}$ according to (6b). Note that the decoupling matrix $\mathbf{G}$ is non-singular because of $0 \leq \bar{s} \leq l$.

Post-print version of the article: A. Pfeffer, T. Glueck, F. Schausberger, and A. Kugi, "Control and estimation strategies for pneumatic drives with partial position information", *Mechatronics*, vol. 50, pp. 259–270, 2018. DOI: doi.org/10.1016/j.mechatronics.2017.09.012
The content of this post-print version is identical to the published paper but without the publisher's final layout or copy editing.

The servo compensation is once again given by (6c) and (6d). The term β in (7a) is chosen as

$$\boldsymbol{\beta} = \begin{bmatrix} \ddot{w}_1^d - b_{1,0}\ddot{\epsilon}_1 - b_{1,1}\dot{\epsilon}_1 - b_{1,2}\epsilon_1 - b_{1,3}\int_0^t \epsilon_1 \,\mathrm{d}\tau \\ \dot{w}_2^d - b_{2,0}\epsilon_2 - b_{2,1}\int_0^t \epsilon_2 \,\mathrm{d}\tau \end{bmatrix} , \quad (7c)$$

with the reference trajectories w_i^d, the errors $\epsilon_i = w_i - w_i^d$, and the constant controller parameters $b_{i,j} > 0$. Note that the derivatives $\ddot{w}_1$ and $\dot{w}_2$ are determined using (2) and the velocity $\dot{w}_1$ is calculated by numerical differentiation using a Savitzky-Golay filter, see, e.g., [38, 39]. Application of (7) with (6c) and (6d) to (2) results in a linear and exponentially stable error dynamics.

4. Estimator Design

As described in the introduction, the friction parameters and also the moving mass of a pneumatic drive are not always exactly known. Therefore, a parameter estimator is designed to iteratively adapt the controller parameters. Sampling of (2a) for $t = kT_s, k = 1,2,\ldots$, with sampling time T_s results in the parametric linear model

$$y_k = \mathbf{r}_k^{\mathrm{T}}\boldsymbol{\zeta}, \quad (8a)$$

with output $y_k = \bar{\bar{s}}(kT_s) + g\sin(\varphi)$, parameter vector

$$\boldsymbol{\zeta}^{\mathrm{T}} = \begin{bmatrix} \zeta^1 & \zeta^2 & \zeta^3 \end{bmatrix} = \begin{bmatrix} \frac{1}{m} & \frac{c}{m} & \frac{d}{m} \end{bmatrix} , \quad (8b)$$

and regressor

$$\mathbf{r}_k = \begin{bmatrix} F_p\big(\bar{p}_1(kT_s),\bar{p}_2(kT_s)\big) + F_a \\ -\mathrm{sign}\big(\bar{\bar{s}}(kT_s)\big) \\ -\bar{\bar{s}}(kT_s) \end{bmatrix} . \quad (8c)$$

Note that the sign-function is used instead of the tanh approximation in (2a) for a better distinction between the Coulomb and the viscous friction. Only the pressures and the position can be measured. For calculating the time derivatives $\bar{\bar{s}}$ and $\bar{\bar{\bar{s}}}$, an acausal centred Savitzky-Golay filter is used, see, e.g., [38, 39].

Remark 1. The formulation (8) is based on an analysis of the noise level of the signals $\bar{\bar{s}}, \bar{\bar{\bar{s}}}, \bar{p}_1$, and $\bar{p}_2$. The functional principle of the short-stroke position sensors at hand is based on several hall sensors. From the resulting noisy position signal the first as well as the second time derivative must be determined. To calculate the (higher) derivatives of noisy signals, different strategies are known from literature, see, e.g., [40, 38]. The comparison of an algebraic linear identification, see, e.g., [40] and different types of Savitzky-Golay filters, see, e.g., [38, 39] leads to the implementation of an acausal centred Savitzky-Golay filter with a polynomial order of 3 and a window length of 35 samples. The filter is used to smooth the position and the pressure signals and to calculate the required derivatives. In particular in a horizontal mounting orientation the resulting acceleration shows the highest noise level. This predestines it for the choice of the output y_k in (8), see, e.g., [33]. To further reduce the influence of noise a so called output dead-zone $y_{\min} \leq |y_k|$, see, e.g., [41], with an additional upper constraint, where only measurements $\bar{\bar{s}}_{\min} \leq |\bar{\bar{s}}(kT_s)| \leq \bar{\bar{s}}_{\max}$, with the output $y_k = \bar{\bar{s}}(kT_s) + g\sin(\varphi)$, are considered valid for the estimation, is utilized. As a consequence, the whole estimation stops when no sufficient excitation is measurable, e.g., at standstill.

4.1. Constrained Recursive Least-Squares Algorithm

The parameter estimation is based on a discrete-time constrained recursive least-squares algorithm with an output dead zone, see [41]. In every time step k, new measurement data $\mathbf{r}_k$ and y_k are used to improve the estimate $\hat{\boldsymbol{\zeta}}_k$ of the parameters $\boldsymbol{\zeta} \in \mathcal{X}$, with the feasible set of parameters $\mathcal{X}$. Inspired by the discrete-time constrained recursive least-squares algorithm, see [41], the estimation algorithm is formulated as

$$\mathbf{k}_k = \frac{\mathbf{P}_{k-1}\mathbf{r}_k}{q + \mathbf{r}_k^{\mathrm{T}}\mathbf{P}_{k-1}\mathbf{r}_k} \quad (9a)$$

$$\mathbf{P}_k = \begin{cases} \left(\mathbf{P}_{k-1} - \mathbf{k}_k\mathbf{r}_k^{\mathrm{T}}\mathbf{P}_{k-1}\right)\frac{1}{q} & \text{for} \quad \hat{\boldsymbol{\zeta}}_{k-1} \in \mathcal{X} \\ \mathbf{P}_{k-1} & \text{else} \end{cases} \quad (9b)$$

$$\hat{\boldsymbol{\zeta}}_k = \mathrm{P}_{\mathcal{X}}\left(\hat{\boldsymbol{\zeta}}_{k-1} + \mathbf{k}_k\left(y_k - \mathbf{r}_k^{\mathrm{T}}\hat{\boldsymbol{\zeta}}_{k-1}\right)\right) \quad (9c)$$

with the forgetting factor $q \in [0,1]$, the matrix[4] $\mathbf{P}_k$, and the orthogonal projection operator $\mathrm{P}_{\mathcal{X}}$. In the practical application, the constraints are known for the physical parameters, i.e., $m \in [m_{\min},m_{\max}]$, $c \in [c_{\min},c_{\max}]$, and $d \in [d_{\min},d_{\max}]$. Hence, the feasible set $\mathcal{X}$ for $\boldsymbol{\zeta}$ takes the form

$$\begin{aligned} \mathcal{X} = \{\boldsymbol{\zeta} | \zeta^1 &\in [1/m_{\max},1/m_{\min}], \\ \zeta^2 &\in [\zeta^1 c_{\min},\zeta^1 c_{\max}], \\ \zeta^3 &\in [\zeta^1 d_{\min},\zeta^1 d_{\max}]\}. \end{aligned} \quad (10)$$

The corresponding projection operator reads as

$$\mathrm{P}_{\mathcal{X}}^{\mathrm{T}}(\boldsymbol{\zeta}) = \begin{bmatrix} \mathrm{P}_{\mathcal{X}}^1(\zeta^1) & \mathrm{P}_{\mathcal{X}}^2(\zeta^1,\zeta^2) & \mathrm{P}_{\mathcal{X}}^3(\zeta^1,\zeta^3) \end{bmatrix} \quad (11a)$$

with

$$\mathrm{P}_{\mathcal{X}}^1(\zeta^1) = \begin{cases} 1/m_{\max} & \text{for} \quad \zeta^1 < 1/m_{\max} \\ \zeta^1 & \text{for} \quad \zeta^1 \in [1/m_{\max},1/m_{\min}] \\ 1/m_{\min} & \text{for} \quad \zeta^1 > 1/m_{\min} , \end{cases} \quad (11b)$$

$$\mathrm{P}_{\mathcal{X}}^2(\zeta^1,\zeta^2) = \begin{cases} \zeta^1 c_{\min} & \text{for} \quad \zeta^2 < \zeta^1 c_{\min} \\ \zeta^2 & \text{for} \quad \zeta^2 \in [\zeta^1 c_{\min},\zeta^1 c_{\max}] \\ \zeta^1 c_{\max} & \text{for} \quad \zeta^2 > \zeta^1 c_{\max} , \end{cases} \quad (11c)$$

[4] The matrix $\mathbf{P}_k$ is sometimes denoted as covariance matrix due to the similarity in stochastic theory.

Post-print version of the article: A. Pfeffer, T. Glueck, F. Schausberger, and A. Kugi, "Control and estimation strategies for pneumatic drives with partial position information", *Mechatronics*, vol. 50, pp. 259–270, 2018. DOI: doi.org/10.1016/j.mechatronics.2017.09.012
The content of this post-print version is identical to the published paper but without the publisher's final layout or copy editing.

$$\mathrm{P}^3_{\mathcal{X}}(\zeta^1,\zeta^3) = \begin{cases} \zeta^1 d_{\min} & \text{for} \quad \zeta^3 < \zeta^1 d_{\min} \\ \zeta^3 & \text{for} \quad \zeta^3 \in [\zeta^1 d_{\min}, \zeta^1 d_{\max}] \\ \zeta^1 d_{\max} & \text{for} \quad \zeta^3 > \zeta^1 d_{\max} \ . \end{cases} \tag{11d}$$

Note that Lyapunov stability of the estimation algorithm (9) and (11) cannot be shown in a systematic way. A Lyapunov-stable discrete-time constrained recursive least-squares algorithm is presented in [42]. However, a time-consuming Cholesky decomposition of the matrix $\mathbf{P}_k$ is utilized within this algorithm. The matrix $\mathbf{P}_k^{-\frac{1}{2}}$ is then used to map the estimated parameters and the constraints.

4.2. Master-Slave Scheme

For the estimation of $\hat{\boldsymbol{\zeta}}$ always a trade-off has to be found between fast convergence, which requires small values of the forgetting factor q, and estimation robustness with respect to noisy data, resulting in large values of $q \in [0,1]$. To resolve this problem, a master-slave scheme is introduced, where two recursive least-squares algorithms with identical models are used in parallel. Similar approaches can be found in literature, see, e.g., the AFMM approach from [43], where multiple models are used, or the survey paper [44]. The working principle of the master-slave approach is shown in Fig. 10. Here, two equivalent estimators are implemented, and after a given number of valid measurements, the norms of the residuals $y_k - \mathbf{r}_k^{\mathrm{T}}\hat{\boldsymbol{\zeta}}$ are compared. The one with the lower residual is set as master and its estimated parameters are used to parametrize the controllers. The one with the larger residual (the slave) is then reset. As a consequence, the initial parameters $\hat{\boldsymbol{\zeta}}_0$ are set to the current estimation of the master, the matrix $\mathbf{P}$ is reset to $\mathbf{P}_k = \mathbf{P}_0$ and the internal memory of the Savitzky-Golay filters is cleared. This leads to fast convergence of the slave due to the large entries in $\mathbf{P}_0$. Note that even if the residuals are, after a given amount of valid data points, equal, which is the case at the initial start, one of the estimators is reset.

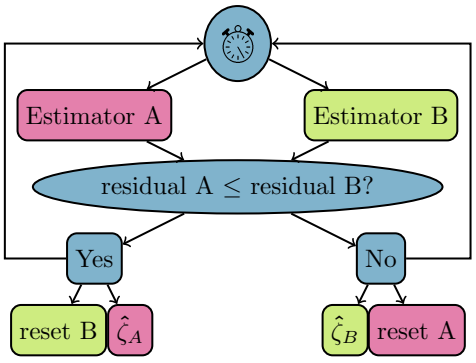

Figure 10: Working principle of the master-slave estimation scheme.

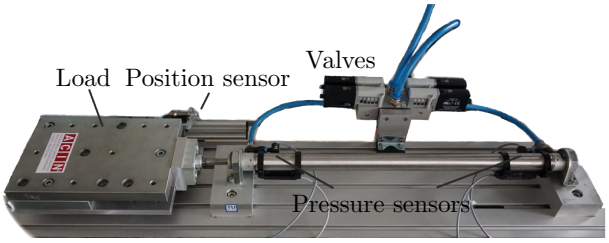

Figure 11: Picture of the horizontal lab test bench.

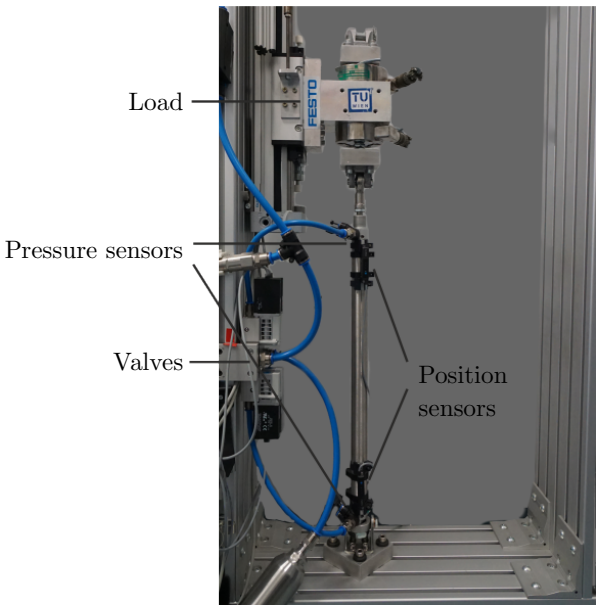

Figure 12: Picture of the vertical lab test bench.

5. Measurements

In the following, measurements from two different test benches are shown. The test benches primarily differ in the mounting orientation, one with a horizontal, see Fig. 11, and another one with a vertical mounting orientation, see Fig. 12. Both use the same industrial standard pneumatic drive DNSU-25-400-PPV-A from Festo, which is a standard part and not a special low friction unit. Note that for all presented measurements the built-in pneumatic dampers (PPV) are deactivated. Four fast switching valves Festo MHA3-MS1H-3/2G-3-K are used to control the pneumatic drive. The low cost Festo SPTE-P10R-S6-V-2.5K pressure sensors are chosen for the pressure measurements. At each end stop of the drive, the position is measurable in a range of about 50 mm. For this, the vertical test bench is equipped with two Festo SDAT-MH5-M50-1L-SA-E-0.3-M8 position sensors. For validation purposes, an additional full-stroke position sensor MTS Sensor Temposonics® R-series is installed at each test bench. Due to different sliders, the friction of the vertical test bench differs from the horizontal one.

Post-print version of the article: A. Pfeffer, T. Glueck, F. Schausberger, and A. Kugi, "Control and estimation strategies for pneumatic drives with partial position information", *Mechatronics*, vol. 50, pp. 259–270, 2018. DOI: doi.org/10.1016/j.mechatronics.2017.09.012
The content of this post-print version is identical to the published paper but without the publisher's final layout or copy editing.

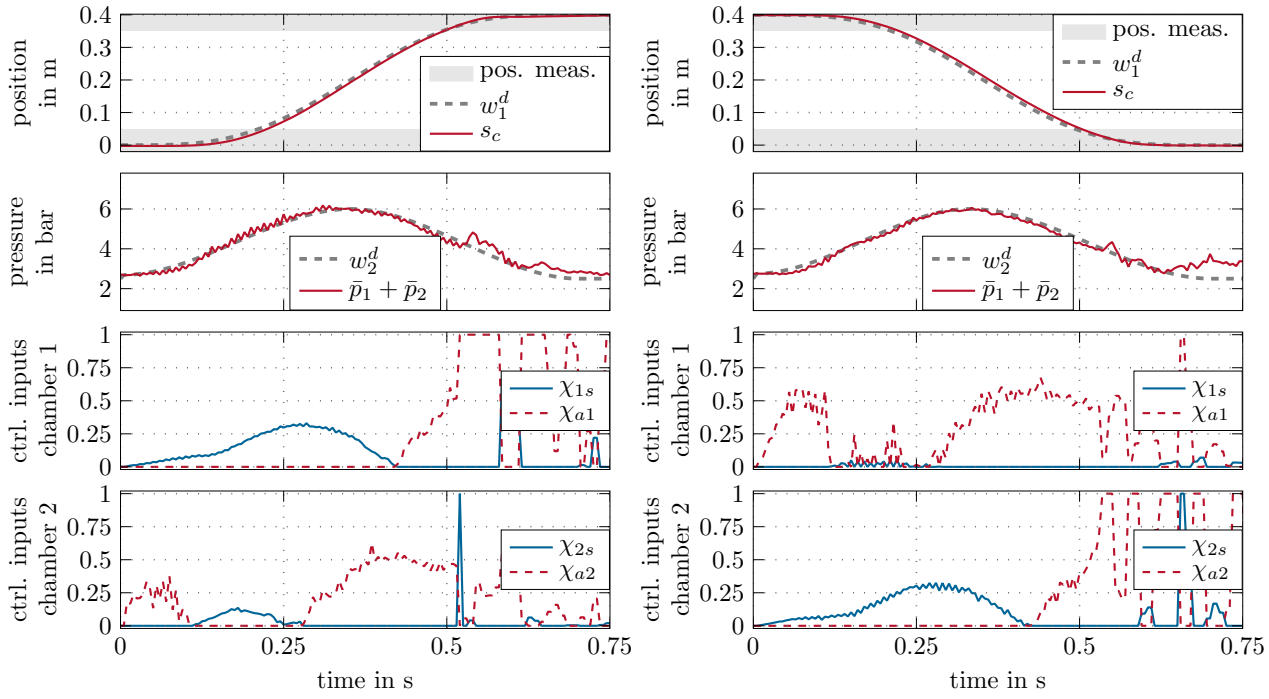

Figure 13: Measurement results for the extension and retraction of the piston rod.

5.1. Soft Landing

The soft landing strategy presented in Section 3 with nominal mass and friction parameters is experimentally validated on the horizontal test bench. The tuning parameters of the trajectory planning are listed in Table 2. Figure 13 gives measurement results for the extension and retraction of the piston rod. On top, the measured piston position s_c and the corresponding desired flat output w_1^d as well as the sum of the chamber pressures $\bar{p}_1 + \bar{p}_2$ and its desired trajectory w_2^d are shown. The bottom of this figure depicts the time evolutions of the control inputs $\chi_{1s}, \chi_{a1}, \chi_{2s}$ and χ_{a2}. The gray background at the top and the bottom in the position measurement indicate the position measurement range. The control approach from Section 3.4 is used to control the piston position and the chamber pressures when the position measurement range is reached. The controller parameters according to (7c) are designed by using pole placement. The poles for the position controller are all set to $-21\,\mathrm{s}^{-1}$ and for the sum pressure to $-1\,\mathrm{s}^{-1}$. The position reference trajectory is determined by the trajectory planning algorithm from Section 3.2. The trajectory of the desired sum pressure results from the trajectory planning strategy presented in [31]. Due to the pressure control during the movement between the position measurement ranges, the sum pressure error is small and there is no need for a new pressure trajectory planning. This is in contrast to the position, where the first available measurements are used to approximate the entry velocity v_0. The initial acceleration a_0 is taken from the originally planned trajectory, because the noisy position signal and the low number of available data points make it impossible to perform a further numerical time differentiation of the velocity signal. Although only the pressure control is active between the position measurement ranges, the measured piston position coincides very well with the desired position trajectory in the nominal case. This indicates a good match of the mathematical model of the mechanical subsystem with reality. Switching from pure pressure control to combined pressure and position control can be easily seen at the inputs. Figure 14 shows a detailed view of the end regions of the cylinder. The dashed lines on the top refer to the desired trajectories. The extension and the retraction movement are depicted on the left and the right hand side, respectively. A comparison of the gray dotted lines from the feedforward control (superscript ^{d,ff}) with the solid lines from the measurements reveal higher velocities of the piston than initially planned. At $t \approx 0.52\,\mathrm{s}$ for the extension and at $t \approx 0.53\,\mathrm{s}$ for the retraction, the initial conditions are approximated and the desired trajectories from Section 3.2 can be calculated (superscript ^{d,si}). From now on, the position control is active. The maximum position errors in the measurement range are about 4 mm for the extension and 3 mm for the retraction, which is quite small for pneumatic systems. Comparisons with alternative trajectory planning strategies, like different filtering approaches, lead to significantly higher maximum errors.

Post-print version of the article: A. Pfeffer, T. Glueck, F. Schausberger, and A. Kugi, "Control and estimation strategies for pneumatic drives with partial position information", *Mechatronics*, vol. 50, pp. 259–270, 2018. DOI: doi.org/10.1016/j.mechatronics.2017.09.012
The content of this post-print version is identical to the published paper but without the publisher's final layout or copy editing.

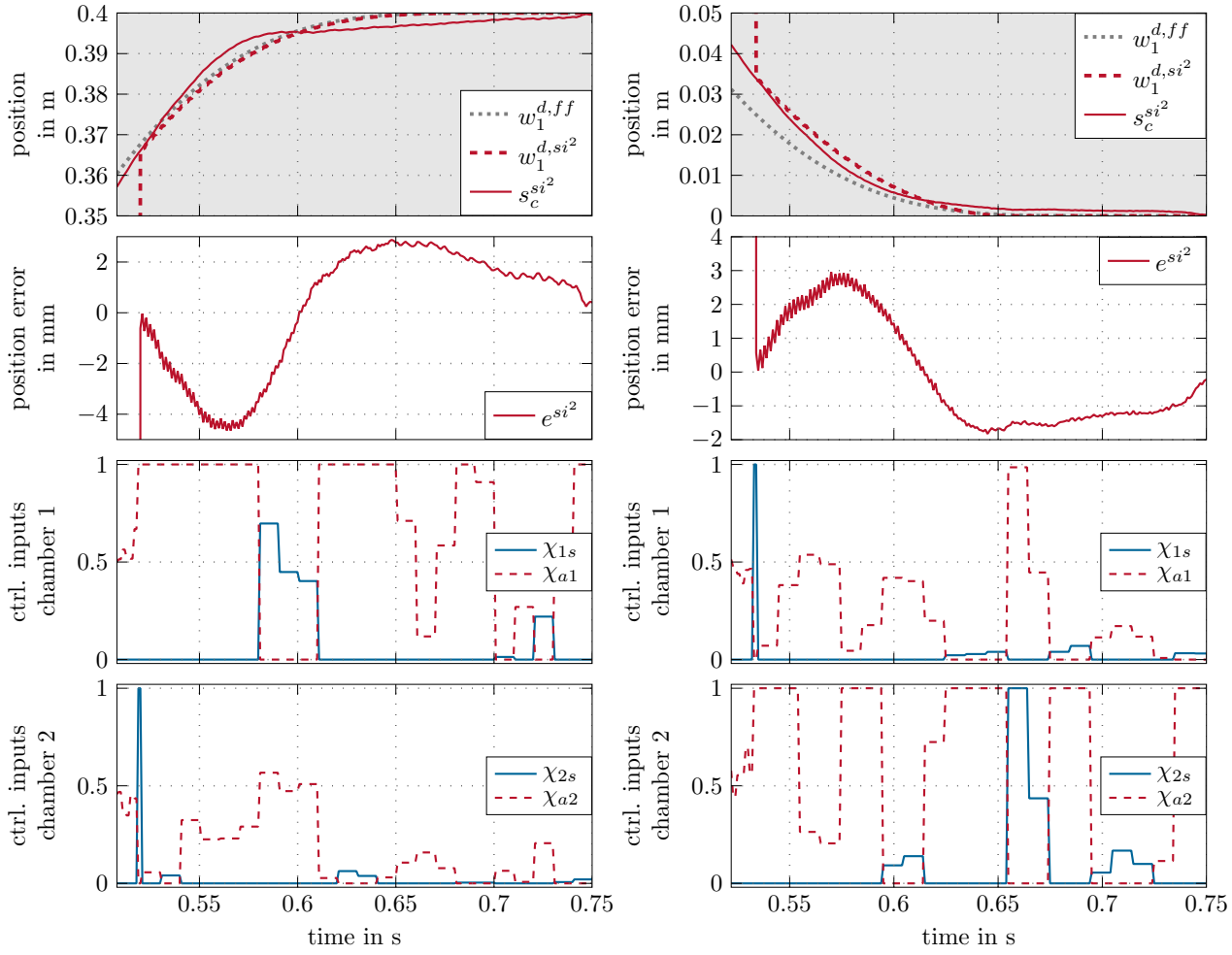

Figure 14: Detailed view of the measurement range at the end stroke from Figure 13.

A better performance of the controller seems to be hard to achieve with the given equipment due to the fact that the controls are temporarily on their bounds. For the retraction movements, the non-modelled direction dependent friction leads to different initial conditions compared to the extension movement, see Table 3. In this case, calculating a new trajectory for the controller is essential for a soft landing of the piston. The extension and the retraction movements show the robustness of the non-overshooting sine-squared approach with respect to varying entry conditions. The proposed trajectory planning in combination with the position control ensures a soft landing of the drive.

5.2. Parameter Estimation

For the validation of the estimation approach, firstly a comparison of a single recursive least-squares estimator with the presented master-slave estimation concept is performed. In a second step, the feedback is closed so that the estimated parameters are used for the online trajectory planning as well as for the model-based controllers. For the following experiments, the tuning parameters of the estimators are chosen as $q = 0.999999$ and $\mathbf{P}_0 = \mathbf{I}$. A sampling rate of 1 ms ensures that the centred Savitzky-Golay filter does not cause recognizable delays in the presented measurements.

Parameters for the trajectory planning

variable	value	description
T	0.75 s	Transition time from one end stop to the other
$\lvert\ddot{s}_{\min}\rvert$	10 m/s^2	Approximation of the minimum acceleration
$\lvert\dddot{s}_{\min}\rvert$	700 m/s^3	Approximation of the minimum jerk

Table 2: Tuning parameters.

Post-print version of the article: A. Pfeffer, T. Glueck, F. Schausberger, and A. Kugi, "Control and estimation strategies for pneumatic drives with partial position information", *Mechatronics*, vol. 50, pp. 259–270, 2018. DOI: doi.org/10.1016/j.mechatronics.2017.09.012
The content of this post-print version is identical to the published paper but without the publisher's final layout or copy editing.

Initial conditions for the non-overshooting trajectory

value	extension	retraction
Δs^d	0.0365 m	0.0344 m
$\lvert v_0 \rvert$	0.48 m/s	0.39 m/s
$\lvert a_0 \rvert$	4.83 m/s^2	4.37 m/s^2

Table 3: Initial conditions of the trajectory planning algorithm for the measurement shown in Fig. 13 and 14.

The advantages of the master-slave scheme are demonstrated by simulation studies. The inputs for these simulations are measurement data taken from the horizontal lab test bench. For comparable results with the vertical test bench, only the first and the last 50 mm of the measurement range of the mounted MTS Sensor are taken into account. For this simulation study, the output dead-zone is chosen as $|\ddot{\bar{s}}_{\min}| = 1.8\,\mathrm{m/s^2}$ for the lower and $|\ddot{\bar{s}}_{\max}| = 60\,\mathrm{m/s^2}$ for the upper constraint. The resulting position and pressure measurements serve as a basis for analyzing the estimation results of a single recursive least-squares estimator with projection as presented in Section 4.1 and a combination of two recursive least-squares estimators as given in Section 4.2. The results are depicted in Fig. 15. The single estimator is indexed with *Sproj* while the master-slave estimator with projection is referred to with the index *ABproj*. The light gray areas in the first part of the figure indicate the measurement range, while the dark gray areas show the chosen box constraints for the parameter estimation. For the first cycles, where the moving mass is $m = 2.1\,\mathrm{kg}$, the results of both estimators are similar. At $t = 10\,\mathrm{s}$ and $t = 100\,\mathrm{s}$, an additional mass is mounted, so that the moving mass is equal to $m = 9.6\,\mathrm{kg}$ and $m = 16.6\,\mathrm{kg}$. From the bottom of Fig. 15, the resets and role changes between master and slave can be identified. As a consequence of the shorter memory of the slave, the change in the mass from $m = 16.6\,\mathrm{kg}$ to $m = 9.6\,\mathrm{kg}$ at $t = 165\,\mathrm{s}$ can be identified much faster with the master-slave approach. The switching from master to slave and vice versa takes place just after two cycles of movement. The same behaviour can be seen at $t = 265\,\mathrm{s}$ when the last mass is unmounted. The single recursive least-squares approach estimates an even bigger mass. When the last additional mass is unmounted all projections are active for the single estimator concept. Note that for the single estimator concept only projection and freezing of the matrix $\mathbf{P}_k$ is realized for the single estimator. This is why, even during the last few cycles of movement the estimated parameters of the single estimator stick on their bounds. A remedy for this may be realized by a heuristic law for a reset of the single estimator concept when all projections are active for a certain time. In contrast, the master-slave estimation approach uses the projection only for short times usually after switching the master-slave roles. The presented measurement results from the horizontal test bench clearly point out the advantages of the master-slave concept compared to the classical single recursive least-squares estimator.

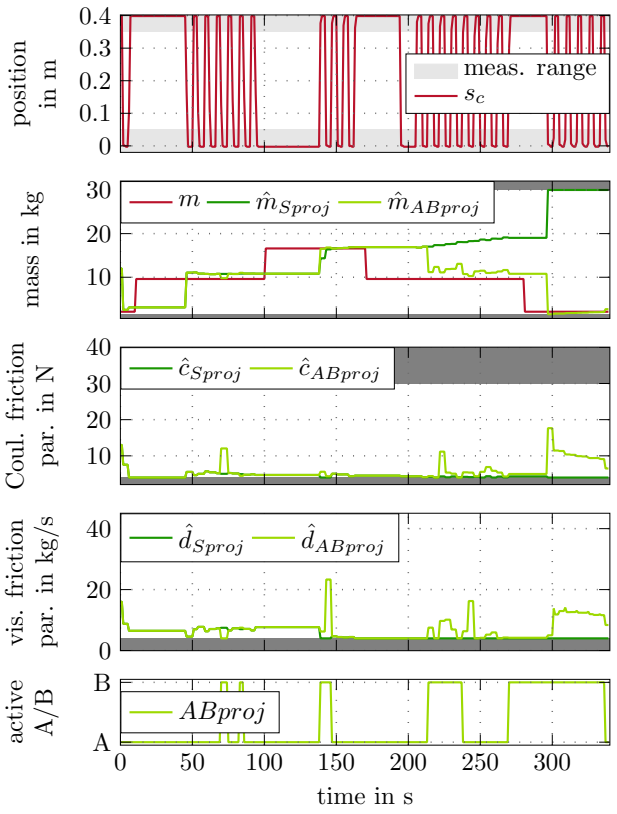

Figure 15: Comparison of the estimation results of a single recursive least-squares estimator with the presented master-slave principle.

5.3. Overall Control Concept

So far, all movements are realized with nominal parameters. In the following, an experiment from the vertical lab test bench, see Fig. 12, is analyzed where the estimated mass as well as the estimated friction parameters are used for the model based controllers. For this, the actual estimation is adopted for the controllers every time the piston is in the lower position before the extension movement begins. The vertical lab test bench is chosen because in this orientation the impact of wrong parameter estimations is considerably larger compared to the horizontal case. Note that for this measurement the full-stroke MTS Sensor position measurement system is only used for validation purposes. The controller as well as the estimators are only connected with the two short position sensors at the end stops. As a consequence of the different position sensors and the changed orientation, the output dead zone is chosen as $|\ddot{\bar{s}}_{\min}| = 0.2\,\mathrm{m/s^2}$ for the lower and $|\ddot{\bar{s}}_{\max}| \approx 130\,\mathrm{m/s^2}$ for the upper constraint. First, a few cycles with the nominal mass of $m = 6.32\,\mathrm{kg}$ are performed to reach a steady state of the estimator. Then an additional mass of 2.83 kg is mounted, which is dismounted after a number of cycles. The corresponding measurements are depicted in Fig. 16. On top, the position measurement and the measurement areas are shown. The estimated parameters follow below.

Post-print version of the article: A. Pfeffer, T. Glueck, F. Schausberger, and A. Kugi, "Control and estimation strategies for pneumatic drives with partial position information", *Mechatronics*, vol. 50, pp. 259–270, 2018. DOI: doi.org/10.1016/j.mechatronics.2017.09.012
The content of this post-print version is identical to the published paper but without the publisher's final layout or copy editing.

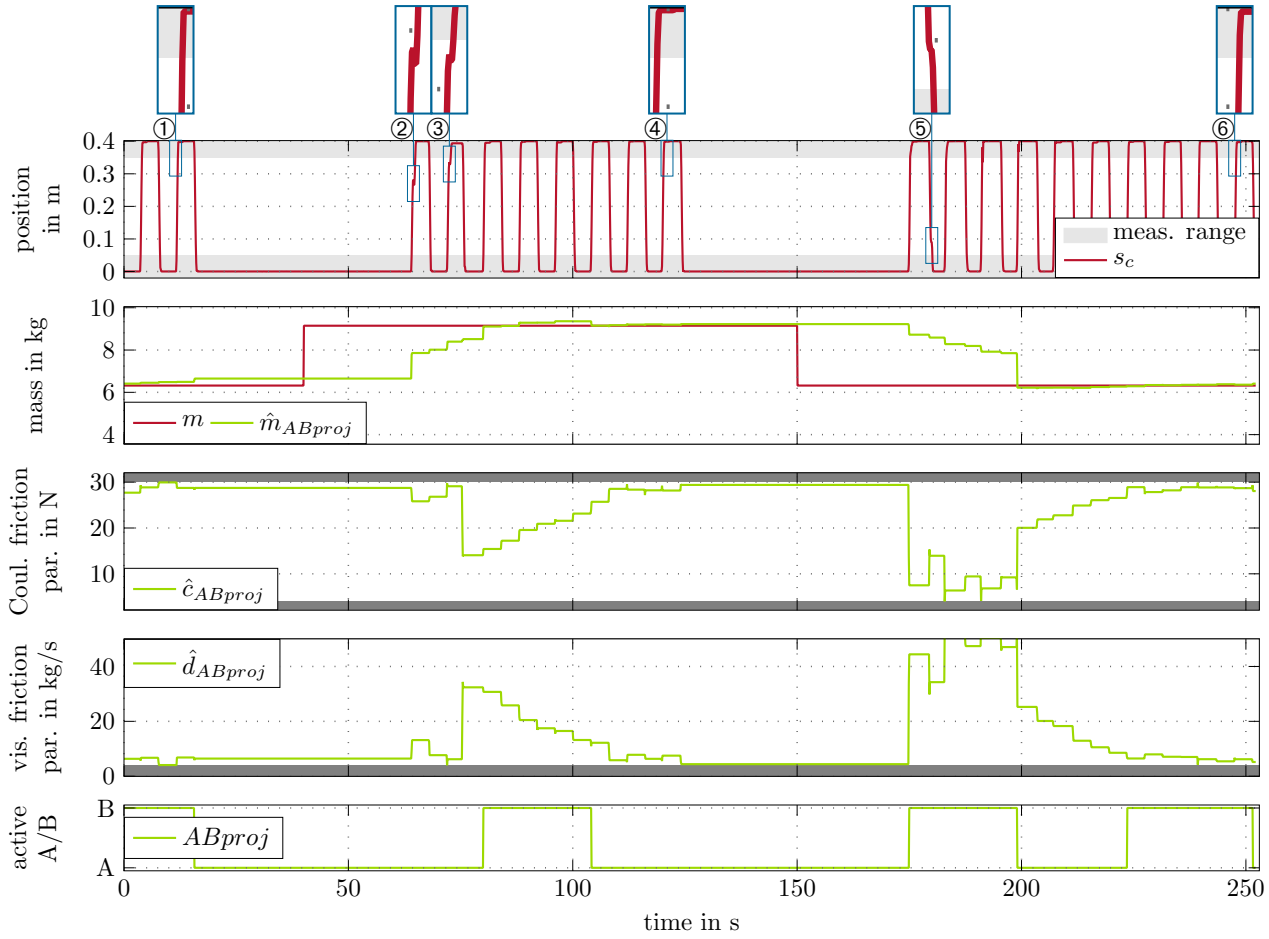

Figure 16: Measurements of the overall system with feedback of the estimated mass and friction. The experiment is performed on the vertical lab test bench of Fig. 12.

The signal at the bottom of the figure indicates the active estimator of the master-slave-scheme. As can be seen at ①, the estimated mass fits the nominal mass very well and the friction parameters allow to smoothly move the drive by the flatness-based feedforward controller. For the next movements beginning with ②, an additional mass of 2.83 kg is mounted. As a consequence, the piston cannot be moved to the opposite measurement area with the nominal trajectory, which is why an auxiliary function is used. After one cycle of movement, the estimated mass is about 8 kg which is not enough for the feedforward controller to reach the opposite measurement area, see ③. In the following cycles, the estimation of the mass and friction parameters exhibit a fast convergence. It can be seen that the estimation converges and that the movement is smoothly preformed with the additional mass mounted. After the movement ④, the additional mass is unmounted. At ⑤, the influence of a too high estimated mass can be seen. The feedforward controller expects a higher gravitational force and therefore the retraction movement cannot be realized. As the measurement results show, the estimation algorithm with the master-slave scheme again provides a fast convergence and all parameters converge to similar values as at the beginning of the experiment, cf. ① and ⑥.

6. Conclusions

This paper deals with the design of control and estimation strategies for a cost-efficient and flexible pneumatic drive system to perform endpoint-to-endpoint movements. The pneumatic drive consists of a differential cylinder, four fast 2-port/2-way switching valves, three pressure sensors, and two short-stroke position sensors near each end stroke. A tailored master-slave estimation scheme, which is based on a constrained recursive least-squares approach, is designed to reliably identify the friction parameters and the moving mass.

The estimated parameters are used to iteratively adopt the model-based controllers. The control concept comprises a controller for the chamber pressure and a combined position and pressure controller which is only active in the position measurement range near the end strokes. Thereby,

Post-print version of the article: A. Pfeffer, T. Glueck, F. Schausberger, and A. Kugi, “Control and estimation strategies for pneumatic drives with partial position information”, *Mechatronics*, vol. 50, pp. 259–270, 2018. DOI: doi.org/10.1016/j.mechatronics.2017.09.012
The content of this post-print version is identical to the published paper but without the publisher’s final layout or copy editing.

the flatness-property of the mathematical model is systematically utilized. Moreover, a non-overshooting trajectory planning algorithm for the piston trajectory was proposed to ensure a soft landing of the piston at the end strokes. The estimation and control concept was implemented on two lab test benches, one with a horizontal, and one with a vertical mounting orientation of the pneumatic drive. Measurement results demonstrate the high performance and the robustness of the proposed approach.

7. Acknowledgements

The authors are very grateful to Festo AG & Co. KG for funding this project.

[1] R. Saidur, N. Rahim, M. Hasanuzzaman, A review on compressed-air energy use and energy savings, Journal of Renewable and Sustainable Energy Reviews 14 (4) (2010) 1135–1153.
[2] M. Doll, R. Neumann, O. Sawodny, Energy efficient use of compressed air in pneumatic drive systems for motion tasks, in: Proc. International Conference on Fluid Power and Mechatronics (FPM), Beijing, China, 2011, pp. 340–345.
[3] X. Shen, J. Zhang, E. J. Barth, M. Goldfarb, Nonlinear model-based control of pulse width modulated pneumatic servo systems, Journal of Dynamic Systems, Measurement, and Control 128 (3) (2006) 663–669.
[4] A. Hildebrandt, R. Neumann, O. Sawodny, Optimal system design of siso-servopneumatic positioning drives, IEEE Transactions on Control Systems Technology 18 (1) (2010) 35–44.
[5] M. Doll, R. Neumann, O. Sawodny, Dimensioning of Pneumatic Cylinders for Motion Tasks, International Journal of Fluid Power 16 (1) (2015) 11–24.
[6] H. K. Lee, G. S. Choi, G. H. Choi, A study on tracking position control of pneumatic actuators, Mechatronics 12 (6) (2002) 813–831.
[7] Y.-C. Tsai, A.-C. Huang, Multiple-surface sliding controller design for pneumatic servo systems, Mechatronics 18 (9) (2008) 506–512.
[8] A. Ilchmann, O. Sawodny, S. Trenn, Pneumatic cylinders: Modelling and feedback force-control, International Journal of Control 79 (6) (2006) 650–661.
[9] E. Richer, Y. Hurmuzlu, A high performance pneumatic force actuator system: Part ii—nonlinear controller design, Journal of Dynamic Systems, Measurement, and Control 122 (3) (2000) 426–434.
[10] S. Hodgson, M. Q. Le, M. Tavakoli, M. T. Pham, Improved tracking and switching performance of an electro-pneumatic positioning system, Mechatronics 22 (1) (2012) 1–12.
[11] S. Hodgson, M. Tavakoli, M. Pham, A. Leleve, Nonlinear discontinuous dynamics averaging and PWM-based sliding control of solenoid-valve pneumatic actuators, IEEE/ASME Transactions on Mechatronics 20 (2) (2015) 876–888.
[12] S. Ning, G. Bone, Development of a nonlinear dynamic model for a servo pneumatic positioning system, in: IEEE International Conference on Mechatronics and Automation, Vol. 1, Niagara Falls, Ontario, Canada, 2005, pp. 43–48.
[13] K. Ahn, S. Yokota, Intelligent switching control of pneumatic actuator using on/off solenoid valves, Mechatronics 15 (6) (2005) 683–702.
[14] P. Beater, Pneumatic Drives, Springer, 2006.
[15] S. Scavarda, Some theoretical aspects and recent developments in pneumatic positioning systems, in: Proc. of the 2nd JFPS International Symposium on Fluid Power, Tokyo, Japan, 1993, pp. 29–48.
[16] H. Hahn, Nichtlineare Regelung eines servopneumatischen Antriebs, at – Automatisierungstechnik 48 (3) (2000) 140–150.
[17] S. Hodgson, M. Tavakoli, M. T. Pham, A. Leleve, Dynamical Model Averaging and PWM Based Control for Pneumatic Actuators, in: Proc. IEEE International Conference on Robotics and Automation (ICRA), Hong Kong, 2014, pp. 4798–4804.
[18] S. Riachy, M. Ghanes, A nonlinear controller for pneumatic servo systems: Design and experimental tests, IEEE/ASME Transactions on Mechatronics 19 (4) (2014) 1363–1373.
[19] P. Rapp, M. Klunder, O. Sawodny, C. Tarin, Nonlinear Adaptive and Tracking Control of a Pneumatic Actuator via Immersion and Invariance, in: Proc. of the 2012 IEEE 51st Annual Conference on Decision and Control (CDC), Maui, Hawaii, USA, 2012, pp. 4145–4151.
[20] A. Toedtheide, T. Lilge, S. Haddadin, Antagonistic impedance control for pneumatically actuated robot joints, IEEE Robotics and Automation Letters 1 (1) (2016) 161–168.
[21] E. Richard, S. Scavarda, Comparison between linear and nonlinear control of an electropneumatic servodrive, Journal of Dynamic Systems, Measurement and Control 118 (2) (1996) 245–252.
[22] W. Gauchel, Energiesparende Pneumatik, Ölhydraulik und Pneumatik O+P 50 (1) (2006) 33–39.
[23] H. Murrenhoff, Grundlagen der Fluidtechnik - Teil 2: Pneumatik, Shaker, 2006.
[24] G. Belforte, S. Mauro, G. Mattiazzo, A method for increasing the dynamic performance of pneumatic servosystems with digital valves, Mechatronics 14 (11) (2004) 1105–1120.
[25] N. Ye, S. Scavarda, M. Betemps, A. Jutard, Models of a pneumatic PWM solenoid valve for engineering applications, Journal of Dynamic Systems, Measurement, and Control 114 (4) (1992) 680–688.
[26] R. van Varseveld, G. Bone, Accurate position control of a pneumatic actuator using on/off solenoid valves, IEEE/ASME Transactions on Mechatronics 2 (3) (1997) 195–204.
[27] D. Schindele, R. Prabel, H. Aschemann, Nonlinear model predictive control of an electro-pneumatic clutch for truck applications, in: Proc. 7th Vienna Conference on Mathematical Modelling (Mathmod), Vienna, Austria, 2012, pp. 526–531.
[28] G. Grzegorz, B. Johann, Minimizing Air Consumption of Pneumatic Actuators in Mobile Robots, in: Proc. IEEE International Conference on Robotics & Automation, New Orleans, LA, USA, 2004, pp. 3634–3639.
[29] H. Keller, R. Isermann, Model-based nonlinear adaptive control of a pneumatic actuator, Control Engineering Practice 1 (3) (1993) 505–511.
[30] W. J. Arteaga-Prez MA, Gutirrez-Giles A, On the observability and the observer design of differential pneumatic pistons, Journal of Dynamic Systems, Measurement, and Control 137 (8) (2015) 0810006–1–081006–25.
[31] A. Pfeffer, T. Glück, A. Kugi, Soft landing and disturbance rejection for pneumatic drives with partial position information, in: Proc. 7th IFAC Symposium on Mechatronic Systems & 15th Mechatronics Forum International Conference, Loughborough, GB, 2016, pp. 559–566.
[32] A. Astolfi, R. Ortega, Immersion and invariance: a new tool for stabilization and adaptive control of nonlinear systems, IEEE Transactions on Automatic Control 48 (4) (2003) 590–606.
[33] L. Ljung, System Identification, Prentice-Hall, 1987.
[34] A. Isidori, Nonlinear Control Systems, 3rd Edition, Springer, 1995.
[35] M. W. Hofmair, M. Melik-Merkumians, M. Böck, M. Merdan, G. Schitter, A. Kugi, Patching process optimization in an agent-controlled timber mill, Journal of Intelligent Manufacturing.
[36] K. L. Knierim, O. Sawodny, Real-time trajectory generation for three-times continuous trajectories, in: 7th IEEE Conference on Industrial Electronics and Applications (ICIEA), Singapore, Singapore, 2012, pp. 1462–1467.
[37] L. Biagiotti, C. Melchiorri, Trajectory Planning for Automatic Machines and Robots, Springer, 2008.
[38] A. Savitzky, M. J. E. Golay, Smoothing and differentiation of data by simplified least squares procedures., Analytical Chemistry 36 (8) (1964) 1627–1639.

Post-print version of the article: A. Pfeffer, T. Glueck, F. Schausberger, and A. Kugi, “Control and estimation strategies for pneumatic drives with partial position information”, *Mechatronics*, vol. 50, pp. 259–270, 2018. DOI: doi.org/10.1016/j.mechatronics.2017.09.012
The content of this post-print version is identical to the published paper but without the publisher’s final layout or copy editing.

[39] R. Schafer, What Is a Savitzky-Golay Filter?, IEEE Signal Processing Magazine 28 (4) (2011) 111–117.
[40] M. Fliess, H. Sira-Ramirez, An algebraic framework for linear identification, ESAIM Control optimisation and calculus of variations 9 (2003) 151–168.
[41] P. A. Ioannou, J. Sun, Robust Adaptive Control, Prentice-Hall, 1996.
[42] G. C. Goodwin, K. S. Sin, Adaptive Filtering Prediction and Control, Prentice-Hall Information and System Sciences Series, Prentice-Hall, 1984.
[43] P. Andersson, Adaptive forgetting in recursive identification through multiple models, International Journal of Control 42 (5) (1985) 1175–1193.
[44] L. Ljung, S. Gunnarsson, Adaptation and tracking in system identification - a survey, Automatica 26 (1) (1990) 7–21.

Post-print version of the article: A. Pfeffer, T. Glueck, F. Schausberger, and A. Kugi, "Control and estimation strategies for pneumatic drives with partial position information", *Mechatronics*, vol. 50, pp. 259–270, 2018. DOI: doi.org/10.1016/j.mechatronics.2017.09.012
The content of this post-print version is identical to the published paper but without the publisher's final layout or copy editing.